Ultrafast THz Probe of Photoinduced Polarons in Lead-Halide Perovskites

Eugenio Cinquanta,[1,2,*] Daniele Meggiolaro,[3,4] Silvia G. Motti,[5] Marina Gandini,[5] Marcelo J. P. Alcocer,[1,6] Quinten A. Akkerman,[7,8] Caterina Vozzi,[2] Liberato Manna,[7] Filippo De Angelis,[3,4,9,†] Annamaria Petrozza,[5] and Salvatore Stagira[1,2]

[1]*Dipartimento di Fisica, Politecnico di Milano, 20133, Milano, Italy*
[2]*Istituto di Fotonica e Nanotecnologie, Consiglio Nazionale delle Ricerche, 20133, Milano, Italy*
[3]*Computational Laboratory for Hybrid/Organic Photovoltaics (CLHYO), Istituto CNR di Scienze e Tecnologie Molecolari (ISTM-CNR), Via Elce di Sotto 8, 06123, Perugia, Italy*
[4]*CompuNet, Istituto Italiano di Tecnologia, Via Morego 30, 16163 Genova, Italy*
[5]*Center for Nano Science and Technology, Istituto Italiano di Tecnologia, 20133, Milano, Italy*
[6]*Solid State Physics and NanoLund, Lund University, P.O. Box 118, SE-221 00, Lund, Sweden*
[7]*Department of Nanochemistry, Istituto Italiano di Tecnologia, Via Morego 30, 16163, Genova, Italy*
[8]*Dipartimento di Chimica e Chimica Industriale, Università degli Studi di Genova, Via Dodecaneso, 31, 16146, Genova, Italy*
[9]*Dipartimento di Chimica, Biologia e Biotecnologie, Università degli Studi di Perugia, Via Elce di Sotto 8, I-06123, Perugia, Italy*

(Received 8 November 2018; revised manuscript received 1 March 2019; published 24 April 2019)

We study the nature of photoexcited charge carriers in $CsPbBr_3$ nanocrystal thin films by ultrafast optical pump-THz probe spectroscopy. We observe a deviation from a pure Drude dispersion of the THz dielectric response that is ascribed to the polaronic nature of carriers; a transient blueshift of observed phonon frequencies is indicative of the coupling between photogenerated charges and stretching-bending modes of the deformed inorganic sublattice, as confirmed by DFT calculations.

DOI: 10.1103/PhysRevLett.122.166601

Metal halide perovskites (MHPs) are "soft-lattice" ionic semiconductors with a direct band gap that present very interesting physical properties including superconductivity, magnetoresistance, ionic conductivity, ferroelectricity, and piezoelectricity, which are of great importance for microelectronics and telecommunication [1]. Recently, metal halide perovskites have been the subject of intensive studies, since they have been identified as the base materials for highly efficient solar cells [2,3].

Despite this active research, there are aspects of the physics of these materials that are still not completely understood. For instance, MHPs behave as defect-free semiconductors with all the scattering processes involving charge carriers mitigated by the screened Coulomb potential, leading to long carrier lifetimes, long diffusion length, and slow electron-hole recombination [4]. Unexpectedly, MHPs show only a moderate carrier mobility that looks conflicting with the previous characteristics. The presence of large polarons—resulting from the dielectric electron-phonon coupling combined with the light effective masses for bare carriers—has been proposed as a possible explanation for the limited carrier mobility in this class of materials [4]. However, no direct experimental fingerprint of the large polaron in the transport properties of MHPs has been reported to date.

In this Letter, by combining ultrafast THz spectroscopy with density functional theory (DFT) calculations, we demonstrate the presence of large polarons in the dielectric response of thin films of $CsPbBr_3$ nanocrystals (a prototypical lead-halide perovskite nanocrystals). We observe a distinctive coupling between the photogenerated charges and dipole-active bending modes of the deformed $PbBr_3$ lattice in the transient THz response. The deviation from a free-carriers dispersion of the transient optical conductivity and the influence of the photoinjected charge on the lattice modes relaxation reveal the polaronic nature of the carriers.

Static and ultrafast THz spectroscopy have been fruitfully adopted for identifying the MHPs low-frequency optical phonons, charge-carrier recombination rates, and hot electron-hole transfer [5–12]. Electronic excitations in most polar semiconductors are strongly coupled to the lattice vibrations. This coupling can lead to carrier trapping or it can induce a certain degree of localization that may result in the formation of polarons, thus changing the nature of the primary generated carrier and affecting transport and recombination mechanisms. Phonon interactions can also strongly perturb the Coulomb correlations between carriers through the modulation of the effective dielectric permittivity, eventually leading to phonon "dressing" of the resultant excitonic states. MHPs are characterized by a small charge carrier effective mass that, in a first approximation, would lead to Bloch states. The softness of the lattice, however, results in a dielectric function that departs significantly from a pure Drude behavior [5–8].

In this framework, the presence of large polarons has been mentioned by Wehrenfennig *et al.* to explain dipole oscillations in the pump-induced THz conductivity spectra [13].

In addition, time-resolved optical Kerr spectroscopy and femtosecond impulsive stimulated Raman spectroscopy allowed us to indirectly address the presence of large polarons in MHPs [14,15].

Here we performed optical-pump THz-probe spectroscopy exploiting our terahertz time-domain spectrometer driven by 25-fs pulses from a 1-kHz Ti:sapphire laser with a center wavelength of 790 nm (1.6 eV). THz pulses with a 0.1–2.7 THz bandwidth were generated and detected by electro-optic sampling in two 1-mm thick ZnTe crystals. For exciting the sample, 400-nm (3.1 eV) laser pulses focused to a spot size diameter of 3 mm at fluences of 85 μJ/cm^2 with a corresponding density of absorbed photons of 5.8×10^{17} photons/cm^3 were used. Our setup can detect a transient dynamic induced in the sample up to a pump-probe delay of about 200 ps.

The investigation was performed on $CsPbBr_3$ nanocrystal thin films. The nanocrystals have been synthesized as reported in Ref. [3] and have an average size of about 30 nm, well beyond the critical size for observing quantum confinement effects. The THz probe pulse has an electric field peak amplitude of tens of kV m^{-1} and about a 1-ps-long optical cycle; thus, it can displace charge carriers on length scales much shorter than the average nanocrystal size. We can therefore consider our outcomes as bulk properties of single crystals. Details concerning the thin film preparation are reported in the Supplemental Material [16].

We first investigated the *static properties* of the perovskite thin films to elucidate the presence of phonons that are expected to be involved in large polaron formation. Figure 1(a) shows the THz probe spectrum and the corresponding measured electric field. Figure 1(b) reports the experimental transmission of the unexcited sample $[T_{\mathrm{Sample}}(\omega)/\mathrm{T}_{\mathrm{Reference}}(\omega)]$. To extract the static dielectric properties of the thin film, this transmission has been fitted with a model transmission obtained by considering the transmission of the THz electric field through the system composed by the thin film and the substrate [17]. Details concerning the THz data extraction are reported in the Supplemental Material [16].

Figures 1(c) and 1(d) show the real part of the refractive index and the absorption spectrum of a 3-μm thick perovskite film in the 10–75 cm^{-1} spectral range acquired at room temperature and extracted from the raw data through the above-mentioned procedure. The refractive index and the absorption spectrum show the presence of four features at 27, 42, 57, and 63 cm^{-1}. Phonon resonances show typical Lorentzian line shapes: the absorption spectrum has a peak in correspondence of each phonon energy, whereas the refractive index shows an inflection point at the same energy. These results agree with previous studies on lead-halide perovskites with different constituents [5–8]. These peaks can be finely retrieved in the DFT-calculated absorption spectrum (dashed red curve) and are related to the superimposition

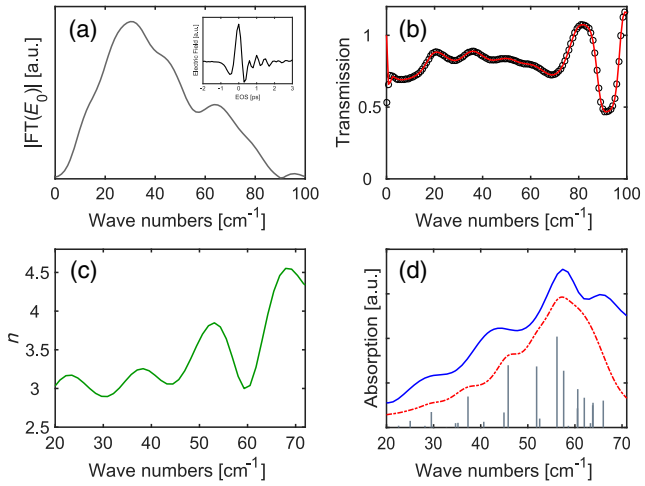

FIG. 1. (a) Probe spectrum used in the optical pump-THz probe experiment with its waveform in the time domain reported in the inset. (b) Experimental transmission of the unexcited sample $T(\omega) = [T_{\mathrm{Sample}}(\omega)/\mathrm{T}_{\mathrm{Reference}}(\omega)]$ (black circle) and corresponding fit with the model transmission (continuous red curve); (c) retrieved real part of the complex refractive index of the sample; (d) calculated IR spectrum (red dashed curve) and experimental (blue continuous curve) THz absorption spectrum of the sample; vertical gray lines are the calculated IR active modes with the related cross sections.

of several IR-active pure bending and mixed stretching-bending modes of the Pb-Br cage [14]. Note that the calculated absorption spectrum shows a good qualitative agreement with the experimental one; however, anharmonicity, local polar fluctuation, dynamic disorder, and cation rotational unlocking are not included in the model. At room temperature, all these contributions can partly affect the phonon frequencies with inhomogeneous peak broadening, resulting in the observed discrepancy between the experimental data and the model [6,20,21]. Dynamic disorder of cations, for instance, plays an important role in soft materials such as organic [22] and ionic semiconductors [20] by modulating many phonon mediated properties, e.g., carrier mobilities.

The large polaron is expected to appear because of coupling of the photoinjected charge with soft lattice phonons [14,23]. Previous ultrafast THz spectroscopy studies of strongly confined ~10 nm large colloidal $CsPbBr_3$ nanocrystals performed in the 0.5–5 THz frequency range reported a Drude response, although just the presence of small oscillations in the transient response [11]. A further study on the same system showed how the transient THz permittivity is characterized by the presence of Lorentzian line shapes that are attributed to the presence of strong carrier-phonon coupling and to a multiphonon process responsible for the hot carrier relaxation [12]. The role of electron-phonon coupling on the pump-induced conductivity has also been studied by THz spectroscopy in $MAPbI_3$ thin films [9,24].

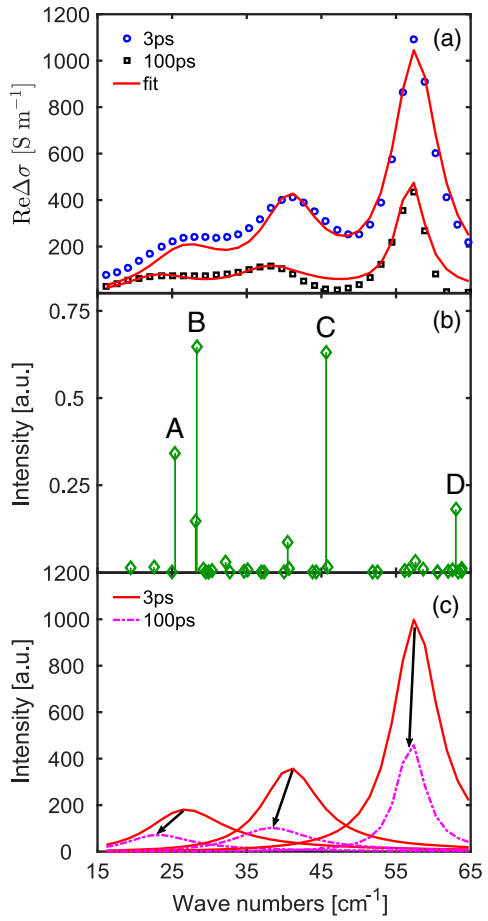

FIG. 2. (a) Transient optical conductivity at 85 μJ/cm^2 (5.6×10^{17} photons/cm^3). Symbols represent the real part of the transient optical conductivity at a pump-probe delay of 3 (blue dots) and 100 ps (black squares), the red lines are the Drude-Lorentz fit of the experimental data. (b) Calculated coefficients of the electron-phonon coupling related to far-IR phonons involved in the large polaron formation; A, B, C, and D are the labels of the most intense phonons mode coupled to the photogenerated carriers. (c) Real part of the Lorentzian fit at 3 and 100 ps (continuous red and dashed magenta lines, respectively).

Remarkably, in our measurements we can clearly identify the large polaron fingerprint in the transient dielectric response of $CsPbBr_3$ nanocrystal thin films. Figure 2(a) reports the transient optical conductivity acquired at 3 and 100 ps after the photoexcitation in the spectral range from 15 to 65 cm^{-1}. Data analysis has been performed with the same retrieval procedure adopted for the static dielectric properties. We observe the presence of three peaks in the real part of the transient optical conductivity spectra. These peaks correspond to inflection points in the imaginary part of the transient optical conductivity and this response clearly indicates the presence of dipole oscillations characterized by Lorentzian line shapes [16]. The red curve in Fig. 2(a) is the fitting of the experimental data with the Drude-Lorentz model $\sigma_f(\omega) = (nq^2/m_p) \cdot (1/\gamma - \imath\omega) + \sum_m [g_m \omega / \imath(\omega_m^2 - \omega^2) + \Gamma_m \omega]$, where n is the density of carriers, q is the elementary charge, m_p is the carrier mass, γ is the scattering rate, g_m is the oscillator strength, Γ_m is the FWHM of the Lorentzian curve, and ω_m *and* ω are the THz angular frequencies of the m phonon and of the probe electric field, respectively. This model hence describes the contribution to the optical conductivity of the polaronic carriers. We adopted $m_p = 3.5 \times m^*$ for the carrier mass ($m^* = 0.21 \times m_e$ is the bare carrier effective mass and m_e is the rest electron mass) in the Drude term to account for the larger mass of the polaronic carriers, as predicted by the Feynman-Osaka model [14,25]. The resulting mobility $\mu = (q\tau_s/m_p)$ of $\sim$60 cm^2/V s (scattering time $\tau_s = 1/\gamma$ $\sim$20 fs as extracted from the Drude-Lorentz fit) is in good agreement with the experimental values reported in the literature [25] and with the predicted upper bound for the polaron mobility of 38 cm^2/V s calculated with the Feynman-Osaka polaron model [14]. In analogy with the MHPs case, crystalline organic semiconductors show absorption features in the far-IR optical conductivity. For this case, the features are due to the interaction between the charge carrier and lattice polarization modes and are described as a harmonic interaction between a fictitious particle and an electron embedded in a viscous fluid, which resemble the large polaron [26]. Recently, an intriguing picture has been proposed to model large polarons in MHPs, beyond the harmonic approximation. As previously discussed, anharmonic effects and dynamic disorder impact the dielectric properties of MHPs, hence leading to complex relationships between the polarization and the external stimulus, in particular near phonon resonances at THz frequencies. Recently, it has been proposed that, due to the anharmonic and dynamically disordered nature of the MHPs lattice, the photoexcitation creates an extra charge with a surrounding local (microscopic) ferroelectric ordering with radial symmetry that couples with low-energy polar phonons to form ferroelectric large polarons [27,28]. Although the Fröhlich formalism, based on the harmonic approximation, nicely describes our experimental results, the inclusion of the dynamic disorder and anharmonic effects in a more accurate model for MHPs should better describe the large polaron dynamics.

To elucidate the nature of the vibrational modes associated with the photoinduced lattice deformations, we analyzed our results with the aid of DFT calculations performed on the orthorhombic phase of $CsPbBr_3$. Details of the calculation are reported in the Supplemental Material [16]. The overall lattice deformation induced by a positive charge within the unit cell was calculated using the hybrid PBE0 functional [29] and fixing cell parameters. The response of the system to the addition of electrons has not been considered here, due to the negligible lattice deformations calculated with both PBE [30] and hybrid PBE0 [29] functionals [14]. The difference of the Cartesian positions of the ions between the neutral and positive energy minima configurations is the variable representing

the lattice distortion. Upon injection of a hole, an average shortening of the Pb-Br bond lengths in the octahedra is reported (−0.04 Å) coupled to an increase of the Br-Pb-Br angle of ∼10° [14,31]. This relaxation stabilizes the lattice by 0.14 eV and pushes the system toward a more "cubic" symmetry, with cations following such a distortion and occupying their corresponding cubic positions in the cell. Based on these observations, the response of the lattice to the positive charge is mainly related to the activation of Br-Pb-Br stretching and bending modes.

Figure 2(b) shows the calculated normalized coefficients of the displacement vectors projected onto the normal modes of the crystal in the relevant spectral region. The most intense displacement activity is predicted for four Pb-Br-Pb pure bending modes at 25, 28, 46, and 63 cm^{-1}, labeled as A, B, C, and D, that are strongly coupled with the injected charge. These values are in very good agreement with the three phonons at 27, 42, and 58 cm^{-1} extracted from the Drude-Lorentz fit of the experimental spectra at 3 ps after the photoexcitation. Indeed, according to the theoretical prediction, these phonon modes are responsible for the formation of the large polaron in the photoexcited lattice. In this respect, we want to highlight that the presence of pump-induced phonon resonances in the transient THz response is not common for nonpolar semiconductors, III-V compounds, and 2D materials. Typical bulk nonpolar semiconductors, like silicon, present a free carrier response [32]. Bulk GaAs, a polar semiconductor, shows a strong coherent coupling of the LO phonon at ∼8 THz with the plasmon through Coulomb interactions and a pure Drude behavior at lower energies (0.5–2.5 THz), while GaAs nanowires show only surface plasmon resonance [33–35]. MoS_2 shows free carriers together with the presence of charged excitons [36]. On the other hand, the lattice softness of lead halide perovskites, 10 times softer with respect to Si and GaAs, is the crucial ingredient for the appearance of the coupling between the photoinjected charge and phonon modes [37].

To gain further insights into the polaronic fingerprint, we analyze the spectra acquired at different pump-probe delays. Figure 2(c) shows the real part of the Lorentzian fits at 3 and 100 ps. At a pump-probe delay of 100 ps, the intensity is decreased, and the phonons are slightly redshifted (24, 40, and 57 cm^{-1}) as compared to the 3 ps delay. This redshift can be explained considering that photogenerated holes in $CsPbBr_3$ nanocrystals distort the PbBr lattice more than electrons [14,31]. Indeed, once the photoexcitation creates a hole in the top of the valence band—which has an antibonding character—the Pb-Br bond becomes stiffer and the lattice shrinks, resulting in a blueshift of phonon frequencies. As the photoinjected charge density starts to decrease, the lattice can expand again, and the Pb-Br bond softens. The observed peak frequencies at 3 and 100 ps in Fig. 2(c) are thus consistent with a lattice compression in the first ps after the photoexcitation and the subsequent expansion during the carrier recombination. Transient optical conductivity spectra at 20 ps after the photoexcitation are shown in the Supplemental Material [16].

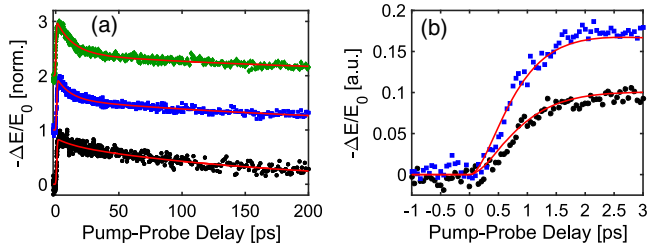

FIG. 3. (a) Transient change of the THz electric field peak transmitted by the $CsPbBr_3$ sample at 0.3 (black dots), 1.1 (blue squares), and 2.2×10^{18} (green diamonds) photons/cm^3 carrier densities together with the biexponential fit (red continuous line). (b) Transient dynamics in the first 3 ps after the photoexcitation at 0.3 and $1.1 \times 10^{18}/cm^3$ (black dots and blue squares, respectively); the red lines are the fit of the buildup dynamics to the rate equation.

If the photoinjected carriers were not coupled to the lattice by the polaron formation, their relaxation would not impact lattice mode frequencies. Given the redshift observed as a function of the pump-probe delay and the agreement between the DFT model and the deconvolution of pump induced conductivity spectra, we claim that the observed features are the fingerprint of the large polaron presence in lead-halide perovskites.

To further explore the carrier dynamics, we studied the frequency-averaged dielectric response of the sample for different optical pump intensities, corresponding to different carrier densities; this response is obtained by recording the transient change of the THz field peak as a function of the pump-probe delay. Figure 3(a) reports the transient electric field $-[\Delta E(t_p, 0)/E_0]$ at pump fluences of 0.3, 1.1, and 2.2×10^{18} photons/cm^3, respectively, where $\Delta E(t_p, 0)$ is the change in the transmitted THz field detected at different pump-probe delays t_p in correspondence of the peak of the THz waveform located at $t_{\mathrm{eos}} = 0$ (t_{eos} is the electro-optical sampling delay) and E_0 is the maximum of the THz field transmitted by the unexcited sample (see Supplemental Material for measurements at 0.07, and 0.8×10^{18} photons/cm^3 [16]). With our experimental setup we are not able to follow the monomolecular decay processes that typically occurs on the ns timescale for this class of materials [3]. Within 200 ps the sample shows an initial fast decay of the transient electric field change with a time constant of about ∼15 ps and a slower one of hundreds of ps [Fig. 3(a)]. The slow component falls well within the band-to-band carrier recombination regime as probed by photoluminescence measurements and often reported in the literature [3]. The fast decay component becomes dominant when the initial carrier density N_0 is larger than $0.5 \times 10^{18}/cm^3$. The relationship between N_0 and the absorbed photon density N_{ph} is calculated as

$N_0 = \varphi 2N_{ph}$, where the photon to carrier ratio was set to $\varphi = 1$. At these densities, trap states are saturated [16] and many-body processes start to play a role; thus this fast dynamic can be assigned to the increase of Augerlike recombination.

Figure 3(b) shows the buildup of the $[\Delta E(t_p, 0)/E_0]$ signal up to 3 ps at 0.3 and 1.1×10^{18} photons/cm^3 (see Supplemental Material [16] for transient optical conductivity spectra in the first 2 ps after the photoexcitation).

The observed formation time is in good agreement with recent outcomes obtained on different perovskite systems. In Ref. [38], a simplified model has been proposed, which considers the initial hot electron cooling and the subsequent large polaron formation, to fit the measured buildup dynamics for different perovskite thin films. The cooling of the hot electron distribution occurs on a subpicosecond timescale and is temperature and excess-energy dependent (τ_{cool}). The large polaron formation, on the other hand, occurs at 400 fs and is temperature and excess-energy *independent* (τ_{pol}). We hence adopt this model and fit the buildup dynamics with a 4 level rate equation system, were the top level A is populated at time 0. Level A and B are blind states to consider cooling and polaron formation; the whole dynamics was fitted using level C population. The formation time τ_{pol} was fixed at 400 fs according to Ref. [38] and the dynamics were convoluted with a Gaussian of 100 fs FWHM (pump pulse duration). The resulting fits are reported in Fig. 3(b) as continuous red curves and nicely describe the experimental data. Within this model we obtain for the cooling time 450 and 540 fs at 0.3 and 1.1×10^{18} photons/cm^3 respectively, in good agreement with the values ($\tau_{cool} \sim 470$ fs) reported for $CsPbI_3$ samples at room temperature and photoexcited by a 400 nm pump [38]. The buildup dynamics measured for the photoconductivity further demonstrate the presence of large polarons in photoexcited perovskites.

In summary, we directly unveiled the presence of large polarons in $CsPbBr_3$ nanocrystal thin films by optical pump-THz probe spectroscopy combined with state-of-the-art DFT calculations. The pump-induced dielectric response of the perovskite thin films is decorated by Lorentzian line shapes that imply the presence of dipole-active vibrational modes coupled to the photoinjected charges due to electron-phonon interaction. Our finding represents a direct experimental evidence of polaronic transport in lead-halide perovskites and can contribute to the understanding of the exceptional physics of these compounds that makes them a rich playground for the implementation of next generation optoelectronics devices.

E. C. thanks D. Viola for the help for the fit of the THz buildup dynamics and R. Sorrentino for support in sample preparation. The Ministero Istruzione dell'Università e della Ricerca (MIUR) and the University of Perugia are acknowledged for the financial support through the program "Dipartimenti di Eccellenza 2018-2022" (Grant AMIS) to F.D.A. E. C., M. J., A. P., and S. S. acknowledge financial support from Fondazione CARIPLO, Project "GREENS" (Ref. No. 2013-0656). E. C., S. S., and C. V. acknowledge funding from the European Research Council Starting Research Grant UDYNI (Grant No. 307964), from the Italian Ministry of Research and Education (ELI project - ESFRI Roadmap) and from Regione Lombardia through the projects FEMTOTERA (ID: CONCERT2014-008) and "Cyber-Sort."

*Corresponding author.
eugenioluigi.cinquanta@cnr.it
†Corresponding author.
filippo@thch.unipg.it

[1] J. Huang, Y. Yuan, Y. Shao, and Y. Yan, Nat. Rev. Mater. **2**, 17042 (2017).
[2] W. Zhang, G. E. Eperon, and H. J. Snaith, Nat. Energy **1**, 16048 (2016).
[3] Q. A. Akkerman, M. Gandini, F. Di Stasio, P. Rastogi, F. Palazon, G. Bertoni, J. M. Ball, M. Prato, A. Petrozza, and L. Manna, Nat. Energy **2**, 16194 (2016).
[4] X.-Y. Zhu and V. Podzorov, J. Phys. Chem. Lett. **6**, 4758 (2015).
[5] S. Zhao, J. M. Skelton, H. Hu, C. La-o-vorakiat, J.-X. Zhu, R. A. Marcus, M.-E. Michel-Beyerle, Y. M. Lam, A. Walsh, and E. E. M. Chia, Appl. Phys. Lett. **111**, 201903 (2017).
[6] C. La-o-vorakiat, H. Xia, J. Kadro, T. Salim, D. Zhao, T. Ahmed, Y. M. Lam, J.-X. Zhu, R. A. Marcus, M.-E. Michel-Beyerle, and E. E. M. Chia, J. Phys. Chem. Lett. **7**, 1 (2016).
[7] M. Sendner, P. K. Nayak, D. A. Egger, S. Beck, C. Müller, B. Epding, W. Kowalsky, L. Kronik, H. J. Snaith, A. Pucci, and R. Lovrinčić, Mater. Horiz. **3**, 613 (2016).
[8] M. Nagai, T. Tomioka, M. Ashida, M. Hoyano, R. Akashi, Y. Yamada, T. Aharen, and Y. Kanemitsu, Phys. Rev. Lett. **121**, 145506 (2018).
[9] C. La-o-vorakiat, T. Salim, J. Kadro, M. T. Khuc, R. Haselsberger, L. Cheng, H. Xia, G. G. Gurzadyan, H. Su, Y. M. Lam, R. A. Marcus, M.-E. Michel-Beyerle, and E. E. M. Chia, Nat. Commun. **6**, 7903 (2015).
[10] T. W. Crothers, R. L. Milot, J. B. Patel, E. S. Parrott, J. Schlipf, P. Müller-Buschbaum, M. B. Johnston, and L. M. Herz, Nano Lett. **17**, 5782 (2017).
[11] G. R. Yettapu, D. Talukdar, S. Sarkar, A. Swarnkar, A. Nag, P. Ghosh, and P. Mandal, Nano Lett. **16**, 4838 (2016).
[12] S. Sarkar, V. K. Ravi, S. Banerjee, G. R. Yettapu, G. B. Markad, A. Nag, and P. Mandal, Nano Lett. **17**, 5402 (2017).
[13] C. Wehrenfennig, G. E. Eperon, M. B. Johnston, H. J. Snaith, and L. M. Herz, Adv. Mater. **26**, 1584 (2014).
[14] K. Miyata, D. Meggiolaro, M. Tuan Trinh, P. P. Joshi, E. Mosconi, S. C. Jones, F. De Angelis, and X.-Y. Zhu, Sci. Adv. **3**, e1701217 (2017).
[15] M. Park, A. J. Neukirch, S. E. Reyes-Lillo, M. Lai, S. R. Ellis, D. Dietze, J. B. Neaton, P. Yang, S. Tretiak, and R. A. Mathies, Nat. Commun. **9**, 2525 (2018).

[16] See Supplemental Material at http://link.aps.org/supplemental/10.1103/PhysRevLett.122.166601 for sample preparation, description of the experimental setup, extraction procedure of the dielectric properties from the raw THz data, and details of the DFT calculations; pump-probe maps at different fluences and transient optical conductivity spectra at different pump-probe delays; and time-resolved photoluminescence data, which includes Refs. [17–19].
[17] L. Duvillaret, F. Garet, and J. L. Coutaz, IEEE J. Sel. Top. Quantum Electron. **2**, 739 (1996).
[18] J. Shamsi, Z. Dang, P. Bianchini, C. Canale, F. Di Stasio, R. Brescia, M. Prato, and L. Manna, J. Am. Chem. Soc. **138**, 7240 (2016).
[19] P. Giannozzi *et al.*, J. Phys. Condens. Matter **21**, 395502 (2009).
[20] O. Yaffe, Y. Guo, L. Z. Tan, D. A. Egger, T. Hull, C. C. Stoumpos, F. Zheng, T. F. Heinz, L. Kronik, M. G. Kanatzidis, J. S. Owen, A. M. Rappe, M. A. Pimenta, and L. E. Brus, Phys. Rev. Lett. **118**, 136001 (2017).
[21] A. M. A. Leguy, A. R. Goñi, J. M. Frost, J. Skelton, F. Brivio, X. Rodríguez-Martínez, O. J. Weber, A. Pallipurath, M. I. Alonso, M. Campoy-Quiles, M. T. Weller, J. Nelson, A. Walshd, and P. R. F. Barnes, Phys. Chem. Chem. Phys. **18**, 27051 (2016).
[22] A. Troisi, Adv. Mater. **19**, 2000 (2007).
[23] M. Schlipf, S. Ponće, and F. Giustino, Phys. Rev. Lett. **121**, 086402 (2018).
[24] M. Karakus, S. A. Jensen, F. D'Angelo, D. Turchinovich, M. Bonn, and E. Cánovas, J. Phys. Chem. Lett. **6**, 4991 (2015).
[25] Y. Chen, H. T. Yi, X. Wu, R. Haroldson, Y. N. Gartstein, Y. I. Rodionov, K. S. Tikhonov, A. Zakhidov, X.-Y. Zhu, and V. Podzorov, Nat. Commun. **7**, 12253 (2016).
[26] G. De Filippis, V. Cataudella, A. S. Mishchenko, N. Nagaosa, A. Fierro, and A. de Candia, Phys. Rev. Lett. **114**, 086601 (2015).
[27] K. Miyata and X.-Y. Zhu, Nat. Mater. **17**, 379 (2018).
[28] P. P. Joshi, S. F. Maehrlein, and X.-Y. Zhu, Adv. Mater. 1803054 (2019).
[29] J. P. Perdew, M. Ernzerhof, and K. Burke, J. Chem. Phys. **105**, 9982 (1996).
[30] J. P. Perdew, K. Burke, and M. Ernzerhof, Phys. Rev. Lett. **77**, 3865 (1996).
[31] F. Ambrosio, J. Wiktor, F. De Angelis, and A. Pasquarello, Energy Environ. Sci. **11**, 101 (2018).
[32] T. Terashige, H. Yada, Y. Matsui, T. Miyamoto, N. Kida, and H. Okamoto, Phys. Rev. B **91**, 241201 (2015).
[33] M. Hase, Appl. Phys. Lett. **94**, 112111 (2009).
[34] Z. Mics, A. D'Angio, S. A. Jensen, M. Bonn, and D. Turchinovich, Appl. Phys. Lett. **102**, 231120 (2013).
[35] H. J. Joyce, S. A Baig, P. Parkinson, C. L. Davies, J. L. Boland, H. H. Tan, C. Jagadish, L. M. Herz, and M. B. Johnston, J. Phys. D **50**, 224001 (2017).
[36] C. H. Lui, A. J. Frenzel, D. V. Pilon, Y.-H. Lee, X. Ling, G. M. Akselrod, J. Kong, and N. Gedik, Phys. Rev. Lett. **113**, 166801 (2014).
[37] Y. Rakita, S. R. Cohen, N. K. Kedem, G. Hodes, and D. Cahen, MRS Commun. **5**, 623 (2015).
[38] S. A. Bretschneider, I. Ivanov, H. I. Wang, K. Miyata, X. Zhu, and M. Bonn, Adv. Mater. **30**, 1707312 (2018).